Detection of the High Eigenmodes of Spin Diffusion in Porous Media

Yi-Qiao Song
Schlumberger-Doll Research, Old Quarry Road, Ridgefield, Connecticut 06877
(Received 7 July 2000)

The dynamics of spin diffusion in a fluid is governed by the Torrey-Bloch equations, and the solution is often expressed mathematically in an eigenmode expansion. We report an experimental demonstration of the excitation and detection of a wide range of eigenmodes in porous media by exploring the inhomogeneous internal magnetic field in the pore space. The nodal character of the eigenfunctions of the high eigenmodes was clearly observed. The methodology of excitation and detection of the high eigenmodes may be used to better characterize pore geometry.

PACS numbers: 66.10.Cb, 05.40.–a, 76.60.–k

The possibility of determining the boundary geometry of a diffusing fluid has been of great mathematical interest [1], as well as physical significance in understanding porous materials. The mathematical solutions of the diffusion equations are often expressed in an eigenmode expansion [2]. The lowest eigenmode can be detected via diffusion and relaxation of spin magnetization [3–5] for the determination of one of the most important length scales, surface-to-volume ratio ($\langle S/V \rangle$) of porous materials. A diffusion propagator can also be used to determine the periodicity and sizes of pores [6–8]. The detection of some of the high modes has been demonstrated recently to determine the multiple length scales existing in sedimentary rocks [9]. It is likely that the properties of the high eigenmodes, such as the spectral density and the functional form of the eigenfunctions, hold the key for a complete characterization of the pore geometry.

In this Letter, we demonstrate the excitation of a wide range of diffusion eigenmodes with the decay time constant (eigenvalues) ranging over 4 orders of magnitude, using a nuclear magnetic resonance technique. In addition, the spatially oscillatory characters of the eigenfunctions of these modes were observed. Our experimental method is simple and can be applied to many porous materials to study pore geometry.

One of the crucial elements of this experiment is the presence of the inhomogeneous magnetic field (B^i) in the internal pore space due to the susceptibility difference between the pore-filling fluid or gas and that of the solid in a uniform external magnetic field [10]. Since it is created by the pore structure, the variation of B^i occurs over the primary length scales of the pore space [11]. The diffusion of a spin inside a pore can then be detected by observing the change of its Larmor frequency, γB^i (γ is the gyromagnetic ratio).

The diffusion of the longitudinal nuclear spin magnetization is governed by the Torrey-Bloch equation [12]

$$\frac{\partial}{\partial t} m(r,t) = D\nabla^2 m(r,t) - \mu m(r,t), \qquad (1)$$

where D is the bulk diffusion constant and μ is the bulk spin relaxation rate. m is the magnetization deviation from its equilibrium. A solution can be found in the general form

$$m(r,t) = e^{-\mu t} \sum_{n=0}^{\infty} A_n \phi_n(r) e^{-t/\tau_n}, \qquad (2)$$

where ϕ_n and τ_n are eigenfunctions and eigenvalues. ϕ_n is normalized: $\int \phi_n(r)^2 \, dr = 1$. The eigenvalues are determined by the boundary condition: $D\hat{n} \cdot \nabla \phi_n = \rho \phi_n$, where $\hat{n}$ is the unit vector normal to surface and ρ is the surface relaxivity. The intensity of each mode is determined by the initial magnetization, $m(r,0)$: $A_n = \int m(r,0)\phi_n(r) \, dr$. It has been shown that the decay rate of the lowest mode is approximately $\rho\langle S/V \rangle + \mu$, while the higher modes are less sensitive to ρ and determined primarily by geometry [3,4,13,14]. Furthermore, $\phi_0(r)$ is approximately a constant throughout the pore, while the high-mode eigenfunctions oscillate [13–15].

A direct way to generate high eigenmodes is to selectively excite spins within a narrow frequency range and the evolution of the Larmor frequency spectrum of these spins is then monitored [16]. Under such selective excitation, $m(r,0)$ is not constant within pores; thus the amplitude of the high eigenmodes can be finite. Consider a spin at r' at time zero. Then, $A_n = \phi_n(r')$. The evolution of this spin is governed by [14]

$$m(r,t;r') = \sum_{n=0}^{\infty} \phi_n(r')\phi_n(r) e^{-t/\tau_n}. \qquad (3)$$

This function is often called the propagator of the magnetization diffusion [10,17].

We assume the excitation is sharp in frequency domain and centered at $f = 0$ [$B^i(r') = 0$]. Thus,

$$m(r,t) = \oint_{B^i(r')=0} dr' \sum_{n=0}^{\infty} \phi_n(r)\phi_n(r') e^{-t/\tau_n}. \qquad (4)$$

This magnetization modulation can be detected by a free-induction-decay (FID) signal: $S(t,t') \equiv \int m(r,t) \times \exp[iB^i(r)t'] \, dr$, as a function of t'. Taking a Fourier transform of $S(t,t')$ with respect to t', and then an inverse Laplace transform with respect to t,

$$\tilde{S}(f,\tau_n) = \langle \tilde{\Phi}_n(f)\tilde{\Phi}_n(0) \rangle, \qquad (5)$$

where $\tilde{\Phi}_n(f)$ is the spectrum of the nth mode:

 0031-9007/00/85(18)/3878(4)$15.00 © 2000 The American Physical Society

$\tilde{\Phi}_n(f) \equiv \int dt' \int dr\, \phi(r) \exp[i(\gamma B^i - 2\pi f)t']$. The angle brackets denote ensemble average as explained below.

Since the excitation is localized in the frequency domain, we make the following assumption about the location of the excitation. Because B^i varies over the pore dimension, the locations with γB^i matching the excitation frequency are isolated lines [11]. Other pores may have a different B^i profile and the excitation locations will be different. Hence, integration over all pores serves as an ensemble average of the location of the initial excitation. The finite frequency width of the excitation pulse limits the highest excited modes to those having a wavelength longer than the size of the excitation spot.

Equation (5) can be simplified for known B^i. For example, if B^i has a constant slope g, then the spectrum $\tilde{S}(f, \tau_n)$ is directly the spatial correlation function of the eigenmodes, $\tilde{S}(f, \tau_n) \propto \langle \phi_n(f/\gamma g)\phi_n(0)\rangle$. This condition is most likely satisfied for small distances and equivalently small frequency shifts.

The nuclear magnetic resonance experiment consists of two radio frequency pulses, inversion and detection pulses, separated by a time t. The magnetization modulation was first created by the inversion pulse, then after time t, inspected by acquiring a FID signal, $S(t, t')$, following the detection pulse. The inversion pulse (t_p) is typically 1 ms long and the detection pulse is 20 μs. The amplitude of the inversion pulse is approximately $1/100$ of the detection pulse. The detection pulse excited the entire resonance line while the inversion pulse excited only a bandwidth of approximately 1 kHz, much narrower than the spectrum width of the sample. The sample used was randomly packed glass beads (Duke Scientific) of 50-μm diam saturated in water in a 5-mm glass tube. The experiments were performed on a Bruker DMX400 spectrometer at a ^{1}H Larmor frequency of 400.1 MHz. The spectral width at half magnitude (FWHM), $\Delta f_0 = 3.5$ kHz, is dominated by the internal field. A series of 100 logarithmically spaced t were used.

The inversion bandwidth was found to vary as a function of t_p, shown in Fig. 1, determined from the spectra (Fig. 1 inset) acquired 0.2 ms after the pulse. We found the narrowest inversion bandwidth at $t_p = 1$–3 ms. This is expected since the spectral width of the pulse and the diffusion distance are dependent on t_p. The broadening due to diffusion during the pulse can be estimated:

$$\Delta f \approx 2\Delta f_0 \frac{\sqrt{6Dt_p}}{d}, \qquad (6)$$

where d is the bead diameter. Thus, including the spectral width ($1/t_p$) of the pulse, the inversion bandwidth is $(\Delta f^2 + 1/t_p^2)^{1/2}$, in good agreement with the data (Fig. 1). The minimum bandwidth should occur at $t_p = (d^2/12\Delta f_0^2 D)^{1/3} \approx 1.9$ ms, also consistent with the data. However, at long time when the diffusion distance is close to d, Eq. (6) will fail and $\Delta f \to \Delta f_0$.

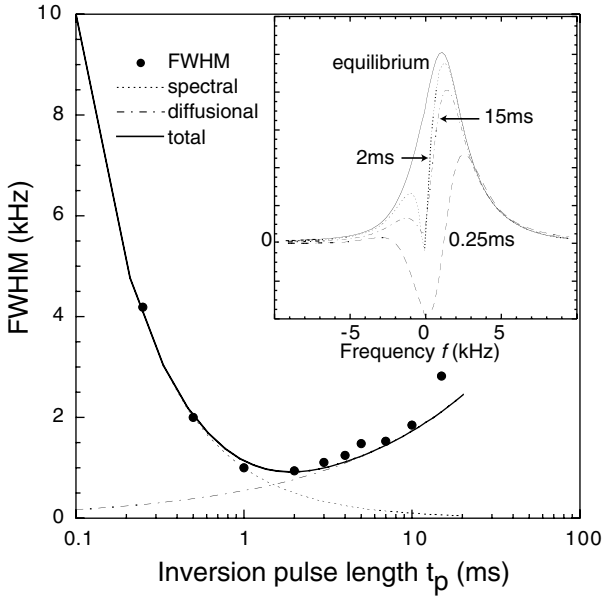

FIG. 1. The FWHM (dot) of the inversion profiles as a function of the inversion pulse length t_p. The sum (solid line) of the spectral (dotted line) and diffusional (dash-dotted line) contributions agrees with the data. Inset: Frequency spectra detected at 0.2 ms after the inversion. t_p is 0.25, 2, and 15 ms as labeled. The equilibrium spectrum is shown as the solid line.

The spectral evolution after the selective inversion was shown in Fig. 2. For the shortest t, the spectrum reflects mostly the profile of the inversion pulse centered at $f = 0$. For short t's, we observed a rapid recovery of the intensity at $f = 0$ and a decrease of the intensities around $f = \pm 1$ kHz, and thus a significant change in the shape of the spectrum. However, the integrated intensity does not change much because t is much less than the spin-lattice

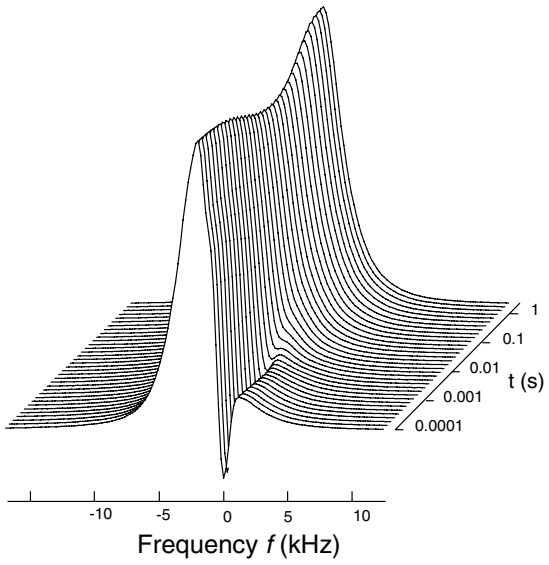

FIG. 2. Frequency spectra detected a t time period after the inversion. The inversion pulse was 1 ms long (t_p) and at zero frequency offset.

relaxation time. This movement of intensities among different parts of the spectrum is unambiguously due to water diffusion. At $t \sim 0.1$ s, the spectral shape returns to approximately that of the equilibrium spectrum, suggesting that the magnetization distribution is mostly uniform within individual pores. This observation indicates that the magnetic field inhomogeneity is over a distance of the order $\sqrt{Dt} \approx 15$ μm, the single pore length scale.

Figure 3 shows the t dependence of signals at several frequencies. At $f = 0$, we observed a monotonic recovery of the signal as a function of t. For frequencies away from zero, the intensity decreases first, e.g., farther away from their equilibrium values, before they recover toward the equilibrium. This indicates that these frequencies represent locations close to the inversion points and the exchange of magnetization occurs via diffusion. Farther away from the center, the signals do not change much as a function of t indicating that those positions are far away from the inversion points and there is no significant exchanges of magnetization through diffusion.

Furthermore, from Fig. 3, it appears that although most of the line shape changes have occurred before $t = 0.1$ s, there is still significant difference between the data at different frequencies up to 2 s, which corresponds to a diffusion distance of almost 200 μm. This indicates that the inversion pulse also excited some long wavelength modes across several pores. These long wavelength modes are not explained by the isolated pore picture outlined by Brownstein and Tarr [15] because the first excited mode would have a time constant of about 0.1 s. Their presence is due to the connectivity of the pores in the packed bead sample and the result of the coupling of modes in the nearby pores. These modes have been studied theoretically [18] and were shown to form a band similar the electron band structure in solids. The decay rate of these modes is $\approx D_{\text{eff}} p^2 + 1/\tau_0$, where p is the wave vector [18].

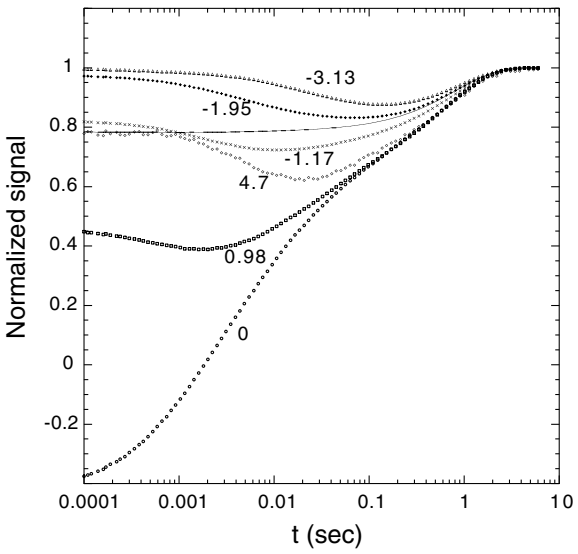

FIG. 3. The recovery of the normalized signals $[S(f,t)/S(f,\infty)]$ for several frequencies as a function of t. The frequency offsets (in units of kHz) are labeled in the graph. The normalized total signal intensity is shown as the solid line.

In order to analyze the character of the diffusion modes quantitatively, we have subtracted the contribution of the lowest mode $[S_0(f,t)]$ from the data. Then, numerical Laplace inversion is performed for each frequency along the t dimension. The transform is done by fitting to the form $\sum a_n \exp(-t/\tau_n)$ using 100 values of logarithmically spaced τ_n. The fit is stabilized by a regularization term and allows both positive and negative amplitudes. The result of the transform is shown in Fig. 4A for the two-dimensional spectrum and several of the slices are shown in Fig. 4B for $\tau_n = 0.0003, 0.002, 0.01, 0.04, 0.2$, and 1 s.

The oscillatory character is evident in Fig. 4. The apparent asymmetry for positive and negative frequencies is due to the inversion frequency being on the high frequency

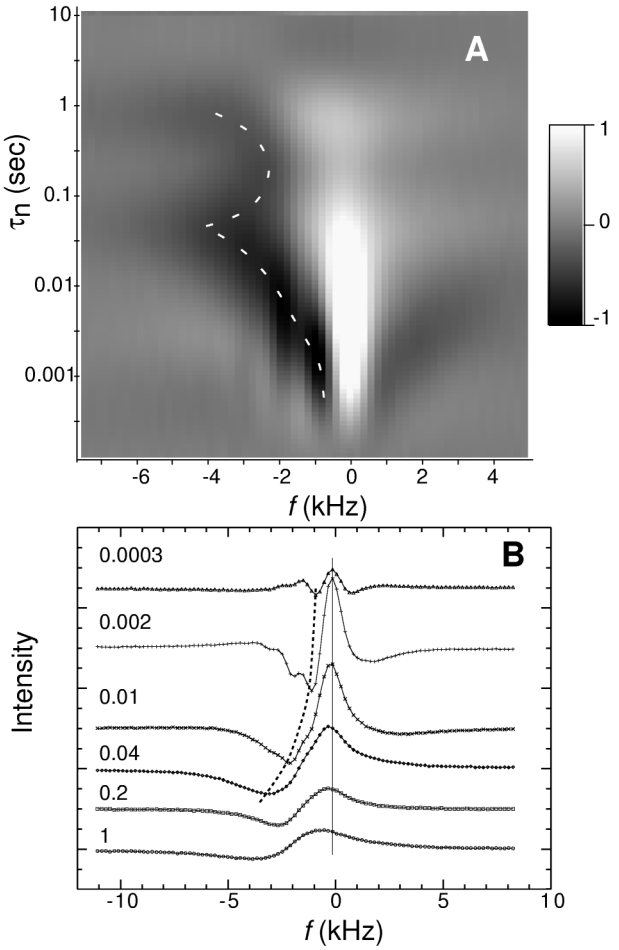

FIG. 4. (A) The two-dimensional spectrum of the diffusion modes, $\tilde{S}(f,\tau_n) - \tilde{S}_0(f,\tau_n)$, excluding the contribution from the lowest modes. The white dashed line illustrates the change in the frequency of the minimum. (B) The frequency spectra of the diffusion modes, $\tilde{S}(f,\tau_n) - \tilde{S}_0(f,\tau_n)$, with $\tau_n = 0.0003, 0.002, 0.01, 0.04, 0.2$, and 1 s. The dashed line goes through the minimum of each spectrum illustrating the changes of the period as a function of τ_n.

shoulder of the spectrum. At $f = 0$, all the coefficients are positive [Eq. (5)]. As f decreases from zero, $\tilde{S}$ decreases and becomes negative. The oscillation occurs for several cycles at small τ_n. The period of this oscillation is related to the spatial period of the specific eigenfunctions, ϕ_n, and the change in the period is clearly shown in Fig. 4 where the modes of short τ_n exhibit more rapid oscillation and the long τ_n modes do slower. This observation confirms that the faster decaying modes are indeed of shorter spatial wavelength. For $\tau_n < 0.001$ s, the position of the negative valley does not appear to change for different τ_n because of the diffusion during the acquisition time of approximately 0.5 ms. This gives the minimum diffusion distance (~ 3 μm) detectable by the current method at this magnetic field.

The period reaches a maximum at $\tau_n \approx 0.03$ s, corresponding to a linear distance of $\pi\sqrt{D\tau_n} = 27$ μm. We speculate that the maximum period occurs when the wavelength of the ϕ_n matches the principle pore dimension, pore size. This is quite consistent with the diameter ($0.828a = 21$ μm) of the largest secondary sphere that can be fit into the close-packed structure [19].

For $\tau_n > 0.04$ s, the period becomes smaller again to $\tau_n = 0.2$ s before it increases for larger τ_n. This part of the spectrum is from the long wavelength eigenmodes [18]. However, the origin of the peculiar change of the period is unclear, possibly related to the semiperiodic nature of B^i. When the wavelength equals the distance between the nearby pores, one might expect that the period along the frequency axis is the minimum. The length scale corresponding to $\tau_n = 0.2$ s is $\pi\sqrt{D\tau_n} = 70$ μm, a distance slightly larger than the bead diameter (50 μm), the periodicity of the pores. When the wavelength is even longer, the excitation intensity of such modes reduces since the spatial Fourier components of the internal field diminishes at such a long wavelength.

In conclusion, the eigenmode spectrum of diffusion embodies the rich details about the boundary geometry and various parts may yield information on the characteristic length scales. This is in close analogy to the case of quantum mechanics where the energy-level spectrum and density of states are considered of prime importance to the understanding of atoms, molecules, and solids. This work demonstrates a simple and general methodology for the manipulation and detection of a wide range of the eigenmodes of diffusion with decaying time constants spanning 4 orders of magnitude ($1-10^{-4}$ s). A better understanding of such eigenmodes may enable a more complete characterization of the pore space in natural and man-made materials.

We thank S. Ryu, P. N. Sen, M. Hürlimann, and C. Straley for numerous discussions and suggestions.

[1] M. Kac, Am. Math. Mon. **73**, 1 (1966).
[2] J. Crank, *The Mathematics of Diffusion* (Oxford University Press, New York, 1999), 2nd ed.
[3] M. H. Cohen and K. S. Mendelson, J. Appl. Phys. **53**, 1127 (1982).
[4] P. G. de Gennes, C.R. Acad. Sci. **295**, 1061 (1982).
[5] W. P. Halperin, F. D'Orazio, S. Bhattacharja, and J. C. Tarczon, in *Molecular Dynamics in Restricted Geometries,* edited by J. Klafter and J. M. Drake (John Wiley & Sons, New York, 1989), Chap. 3.
[6] D. G. Cory and A. N. Garroway, Magn. Reson. Med. **14**, 435–444 (1990).
[7] P. T. Callaghan, A. Coy, D. MacGowan, K. J. Packer, and F. O. Zelaya, Nature (London) **351**, 467–469 (1991).
[8] P. P. Mitra, P. N. Sen, L. M. Schwartz, and P. Le Doussal, Phys. Rev. Lett. **68**, 3555 (1992).
[9] Y.-Q. Song, S. Ryu, and P. N. Sen, Nature (London) **406**, 178 (2000).
[10] P. T. Callaghan, *Principles of Nuclear Magnetic Resonance Microscopy* (Oxford University Press, New York, 1993).
[11] S. Ryu, P. N. Sen, and B. Audoly (private communication).
[12] H. C. Torrey, Phys. Rev. **104**, 563 (1956).
[13] K. R. Brownstein and C. E. Tarr, J. Magn. Reson. **26**, 17–24 (1977).
[14] S. Ryu *et al.* (to be published).
[15] K. R. Brownstein and C. E. Tarr, Phys. Rev. A **19**, 2446 (1979).
[16] The use of a localized excitation was first suggested by S. Ryu and later independently by P. Speier and B. Sun.
[17] J. Kärger and W. Heink, J. Magn. Reson. **51**, 1–7 (1983).
[18] P. N. Sen, L. M. Schwartz, P. P. Mitra, and B. I. Halperin, Phys. Rev. B **49**, 215 (1994).
[19] H. E. White and S. F. Walton, J. Am. Ceram. Soc. **20**, 155 (1937).